dc SQUID Design with Femtotesla Sensitivity for Quantum-Ready Readouts

I. Sochnikov[1,2,*] D. Davino,[1] and B. Kalisky[3,4]

[1]*Physics Department, University of Connecticut, Storrs, Connecticut 06269, USA*
[2]*Instiue of Material Science, University of Connecticut, Storrs, Connecticut 06269, USA*
[3]*Department of Physics, Bar-Ilan University, Ramat-Gan, Israel*
[4]*Institute of Nanotechnology and Advanced Materials, Bar-Ilan University, Ramat-Gan, Israel*

Among some of the current uses of dc superconducting quantum interference devices (SQUIDs) are qubit readouts and sensors for probing the properties of quantum materials. We present a gradiometric niobium SQUID design with state-of-the-art sensitivity in the femtotesla range, which can be tuned to specific readout requirements. The sensor is a next-generation fractional SQUID with a tightly optimized input coil and a combination of various measures known for restraining parasitic resonances and other detrimental effects. Our design combines the practical usefulness of well-defined pickup loops for well-defined imaging kernel and tunable probing applications with a fractionalization approach to reduce undesired inductances. In addition, our modeling predicts small dimensions for these planar sensors. These features make them of relevance for material studies and for the detection of magnetic fields in small volumes, e.g., as part of a cryogenic scanning quantum imaging apparatus for efficient diagnostics and quantum device readouts. This manuscript will benefit scientists and engineers working on quantum-computing technologies by clarifying potential general misconceptions about dc SQUID optimization alongside the introduction of the flexible compact dc SQUID design.

I. INTRODUCTION

Superconducting quantum interference devices (SQUIDs) remain one of the least perturbative and most sensitive magnetic field detection technologies available today. The SQUIDs rely on the property of the singly valued wave function along the SQUID circumference, which leads to its periodicity with flux through the SQUID contour [1]. Nearly any physical property of a SQUID becomes sensitive to flux in a quantized way, allowing it to be used as a sensor of magnetic flux or field. SQUIDs range from large devices used in bulk material characterization, living organism signal detection, and geological systems [1] to submicron-sized sensors [2] at superior signal levels, leading to thrilling discoveries in quantum materials [3–8]. A particularly underexplored area is the utilization of still compact but extremely high field (integrated flux) sensitivity SQUID sensors in a scanning setup. They are ideally suited for challenging applications, such as diagnostics of parasitic surface spins on full-scale wafers of materials (e.g., monolayers) and, even timelier, as nonperturbing qubit readouts

[9–16]. By using a qubit-readout SQUID on a scanning platform [17], a *tunable nonperturbative* electromagnetic quantum coupling may be realized, which is not possible in readouts fabricated on the same chip as the qubit (Fig. 1). Another possible significance of such devices is in quantum-classical interfacing [18], where heat dissipation is removed from a qubit chip by using a remote scanning SQUID, which minimizes back action and minimizes effects from poisoning phonons and quasiparticles [19–21]. Thus, oftentimes, SQUIDs are desirable on a millimetric length scale for nonperturbative adjustable coupling and large-area or large-cross-section field integration for efficient signal collection and reduced effects from polluting processes.

Here, we first review sensitivity concerns in dc SQUIDs and then show modeling and the design of practical gradiometric SQUID sensors for the femtotesla range (Figs. 2–4) for the scanning imaging and probing applications mentioned above, which is a distinct designation from some previous femtotesla designs [22]. Our calculations (Fig. 5) predict a flux noise figure of merit similar to that of high-coherence qubits and devices [23–25], which substantiates the prospective effectiveness of these devices (Fig. 6) for quantum-ready readouts.
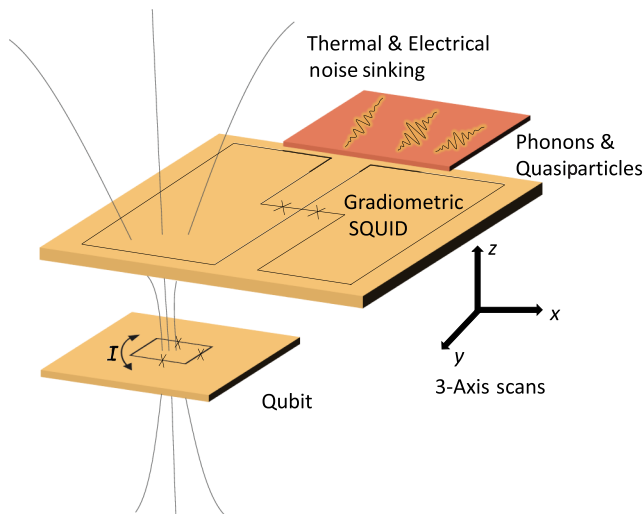
*ilya.sochnikov@uconn.edu

FIG. 1. Scanning SQUID readout of qubits allows for in situ back action and coupling tuning and optimization. Detrimental noise from photons, phonons, and quasiparticles can be efficiently removed in this proposed setup, to enhance qubit coherence (see more details in the Appendix C).

II. SENSITIVITY CONSIDERATIONS FOR dc SQUIDS

The theoretical ultimate energy sensitivity of a simple dc SQUID is determined to be [26–28]

$$\epsilon = \frac{\phi_n^2}{2L} = 16k_B T \sqrt{LC}, \tag{1}$$

where L is the total inductance of the squid loop and C is the capacitance of each Josephson junction, which yields
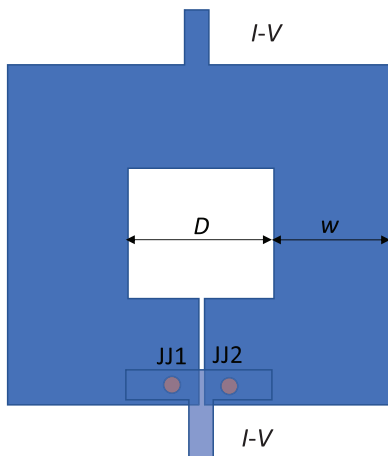

FIG. 2. Square-washer SQUID geometry, which we use as a basic element in our calculations and designs. I-$V+$ and I-$V-$ are biasing leads. JJ1 and JJ2 are Josephson junctions. Square SQUID provides efficient flux collection on a small chip area and efficient coupling to input coils [39].
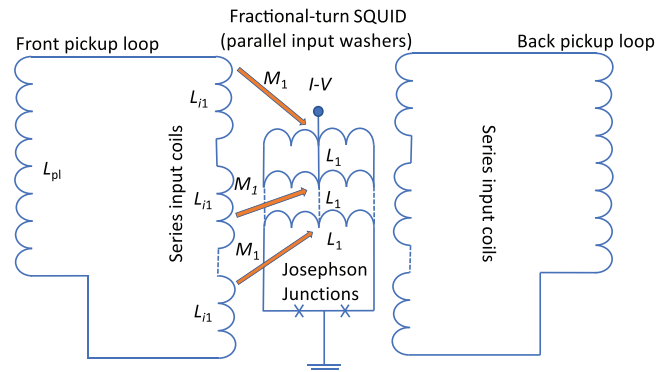

FIG. 3. Simplified circuit diagram of the proposed parallel-washer SQUID gradiometer. Inductance of N input washers of the SQUID is reduced to $L = L_1/N$ due to the parallel connection to obtain $\beta = 1$. Inductance of the input coils adds in series to $L_i = L_{i1}N$ and is equal to the pickup-loop inductance for the most efficient flux transfer. Left and right pickup circuits couple gradiometrically to the external flux. Design includes only two Josephson junctions, but many loops connected in parallel to those junctions. Very efficient flux transformation can be achieved in this way, without compromising the intrinsic noise performance of the SQUID.

the flux noise

$$\phi_n = 4\sqrt{2}(k_B T)^{1/2} L^{3/4} C^{1/4}. \tag{2}$$

This value is the approximate theoretical limit expected with available dc SQUID technologies at finite temperatures (at very low temperatures, there is another quantum-fluctuations term limiting the possible sensitivity [29]). In the current best SQUID systems, the noise level is typically about $10^{-7} - 10^{-6}\Phi_0/\sqrt{Hz}$ [1,7,30–35]. Achieving even these values is not trivial. This figure of merit is relevant to white noise levels at frequencies >10–100 Hz. Below about 10–100 Hz the so-called $1/f$ noise is dominant, but, in particularly carefully fabricated devices, the $1/f$ component is not tremendously high, making the design considerations in this manuscript valid also for low frequencies with somewhat lesser sensitivity (dc limit). Further progress is limited by Josephson-junction technologies and by parasitic noise sources, such as charge noise from the dielectrics and from paramagneticlike spin fluctuations on the surfaces of the metals used in SQUID fabrication [36]. Thus, a very good level of experimental noise is typically about $10^{-6}\Phi_0/\sqrt{Hz}$. Notably, these are white-noise figures and low-frequency $1/f$ noise is typically worse; however, white-noise figures are what are typically referred to in the literature.

The detected external flux couples to the SQUID either directly to the SQUID loop L or through additional superconducting coils, loops, or transformers [37]. As the applied flux ϕ is changed, the current-voltage characteristics of the SQUID oscillates with a period of Φ_0 (the flux
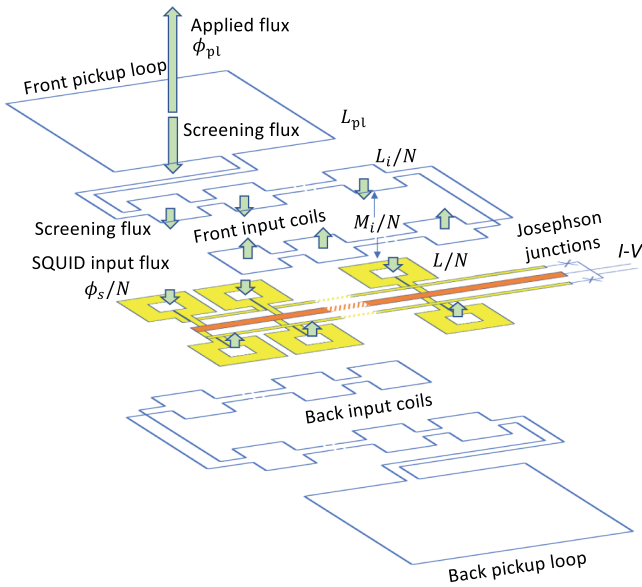
FIG. 4. Wire diagram of our parallel-washer gradiometric SQUID (Fig. 3) unfolded in a three-dimensional schematic. Design implements input coils in series, showing the coupling between different components of the sensor. There are two gradiometrically configured input circuits with pickup loops and N of one-turn input coils connected in series. SQUID consists of N parallel washers configured in a gradiometric fashion. In the actual CAD (computer-aided design), we further improve this approach by reducing the number of turns in the input coils, reducing parasitic capacitances, and implementing damping resistors to reduce resonances.

quantum); the critical current-modulation depth, $\Delta I_M/2I_O$, depends on the important parameter $\beta = 2LI_0/\Phi_0$, which holds information about the modulation depth, where I_O is the zero-flux critical current. For $\beta = 1$, the modulation depth is about 50% or I_0 [30]. Additionally, the current-voltage characteristic is a single value, if another parameter, $\beta_c = 2\pi I_O R^2 C/\Phi_0$, is less than one [38], where R is the junction's shunt resistance. These two parameters define the baseline performance of the SQUID. As a practical rule, the values $\beta \sim 1$ and $\beta_c \lesssim 1$ are used to optimize SQUID performance [26]. Put another way, $I_O R$ should be as large as possible, while keeping $\beta_c \lesssim 1$ and $\beta \sim 1$.

The properties above are strongly dependent on the materials and fabrication process. For a current density of $10\,\mu A/\mu m^2$ in the trilayer Nb/AlOx/Nb process that we use with SeeQC Inc. (formerly Hypres Inc.), the smallest junction radius in our SQUID is about $0.56\,\mu m$, for which we obtain a critical current in the smallest junction of about $10\,\mu A$, a capacitance of about 50fF, and about $5\,\Omega$ shunt resistor, while keeping $\beta_c \lesssim 1$. The condition of $\beta \sim 1$ leads to an optimal inductance of the SQUID of $L = 100\,pF$. In practice, SQUID inductance can be varied by about a factor of two without a realistically noticeable compromise in the performance.

On a more practical level, the geometry of the SQUID plays an important role in noise performance of its field sensitivity (as opposed to flux sensitivity). This geometry defines the inductances of the SQUID and flux pickup circuits, as well as the parasitic inductances and capacitances, which may induce noisy resonances. External and trapped flux rejections are important concerns; flux coupling and flux collection efficiency are also determined by SQUID geometry [39]. Here, we focus our optimization on these parameters and associated designs to achieve high field sensitivity, $B_n = \phi_n/A_{\rm eff}$, where ϕ_n is the intrinsic flux noise of the SQUID defined above and $A_{\rm eff}$ is the effective area of the SQUID, which generally considers flux-focusing and shielding effects [29,39–42]. For square-washerlike SQUIDs (Fig. 2) with $D \gg \lambda$ and $w \gg \lambda$, where λ is the relevant magnetic penetration depth (London or Pearl), the effective area is not the same as the simple geometrical size of the washer and is determined by $A_{\rm eff} \approx D(D + 2w)$. The inductance of this square-washer SQUID is $L = \mu_o(D + w)(2/\pi)\{\ln[1 + (D/w)] + 0.5\}$, for $D/w \geq 10$, and $L = \mu_o D(2/\pi)\{\ln[5 + (D/w)] + 0.25\}$ for $D/w \geq 10$, and $L = 1.25\,\mu_o D$ otherwise [29]. The washer thickness, d, usually enters as a parameter coupled to the penetration depth. The conditions above, $D \gg \lambda$ and $w \gg \lambda$, mean that we assume the thickness of the washer is $d \gg \lambda$. In practice, if we are using niobium layers of a few hundred nanometers thick, with a London penetration depth of about 80 nm and lateral sizes larger than 1–2 μm, the conditions above are well satisfied. Using these expressions, combined with the flux noise expressions above, we calculate the SQUID field sensitivity, as shown in Fig. 5 (note, the approximate, but practically convenient, expressions used for inductances result in artifacts appearing as kinks in the plots). For a SQUID (single, not gradiometer) pickup area of about 5×5 mm^2, signal resolution in the order of 5 fT/$\sqrt{\rm Hz}$ is expected, which makes femtotesla signals attainable within a few seconds of averaging time. However, 1 fT/$\sqrt{\rm Hz}$ requires a much larger pickup area ($\gtrsim 10 \times 10$ mm^2) in this simple geometry.

One intuitive (but typically incorrect) suggestion for improving the field sensitivity of SQUIDs is to increase the number of turns of the SQUID loop, and thus, effectively increase the phase drop (proportional to the flux) on the Josephson junctions. However, the main problem with this solution is that the inductance of the SQUID grows rapidly with the number of turns (usually as the square of the number of turns) and does not outpace the gain from the effective larger pickup (linearly proportional to the number of turns), especially for narrow line loops [43]. This increase happens because the loops must be large (millimeters) for our target field sensitivities, yielding high single-loop inductances. A better strategy is to reduce the detrimental effects of large inductance, rather than only making the SQUID pickup area effectively larger. Notably, while this approach may be useful for
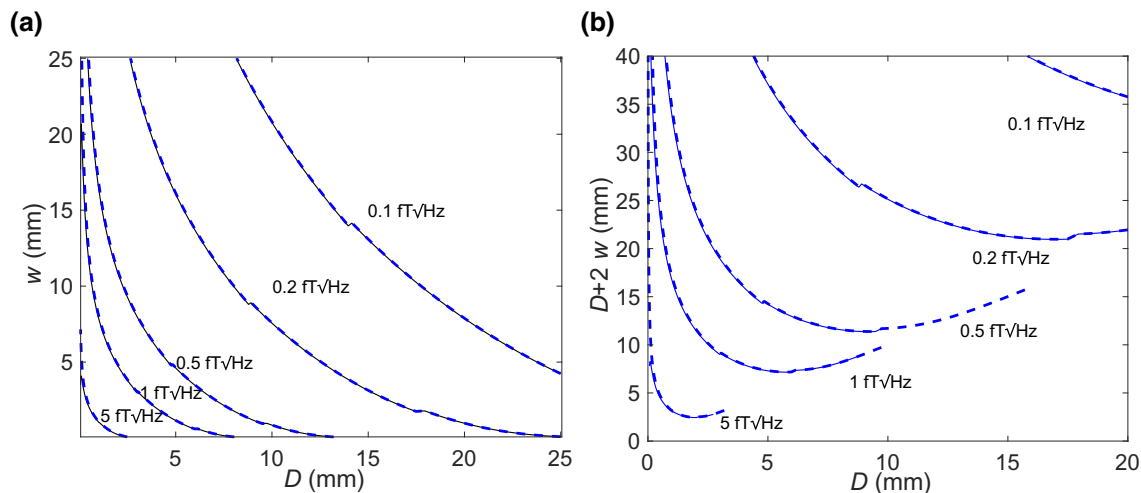
FIG. 5. Sensitivity figures for the Ketchen SQUID (solid line) and fractional-loop washer SQUID (dashed lines) with an input coil. External flux is collected by a pickup loop and through a series of one-turn input coils coupled to the SQUID. (a) Contour plots of the noise in $T/\sqrt{Hz}$ of a SQUID or a pickup loop with an arm width, W, versus the opening size, D. (b) Same sensitivity data plotted as the lateral size of the SQUID versus the SQUID opening size. In bare SQUIDs, to obtain femtotesla sensitivities, SQUIDs should be quite large, more than 20×20 mm^2. In the fractional-loop SQUID, and for realistic fabricated chip sizes of about 10×10 mm^2, we can obtain sensitivities in the range of sub - fT/$\sqrt{Hz}$. Achieving femtotesla range sensitivities is projected with the one-stage input-coil designs; both fractional SQUIDs and Ketchen SQUIDs provide the same expected noise performances.

very small SQUIDs (nano-SQUIDs and micro-SQUIDs) with small inductance, such SQUIDs are not relevant to field-sensitivity devices.

III. FLUX INPUT CONFIGURATION

One way to improve the field performance of the SQUID with direct flux input is to connect several SQUID loops of smaller dimensions side-by-side to increase the overall field collection area and minimize parasitic capacitive coupling [44–50]. In this geometry, the total inductance of the SQUID is about L/N, where L is the individual loop inductance and N is the number of loops. However, improvements in the size of the SQUID are incremental and in the range of a couple of tens of percent reduction (calculated data not shown). This approach usually works well for somewhat less demanding target fields (smaller SQUID pickup area), in this case, the improvement can be more substantial [44–50]. Besides, the multiloop SQUID is not suitable for direct-field imaging of nearby objects due to the complicated imaging kernel of multiple pickup loops. In this section, we rationalize that a different parallel-loop approach can be very useful in SQUIDs with *input-coil circuits*, but not in the direct detection form discussed in the preceding paragraphs.

Generally, the main advantage in using the field coil input circuit is that the large inductance of the input coil can be implemented without a substantial degradation of the SQUID performance. Magnetic field or flux can be collected by a fully superconducting loop of a desired shape and then magnetically (rather than electrically, as in the

direct schemes above) coupled to a SQUID [39]. This approach keeps the SQUID inductance small, while the pickup coil inductance can be larger than that achieved via direct schemes, without a large penalty in intrinsic SQUID noise. However, measures against the effect of parasitic capacitances and inductances that may lead to undesired resonances must be taken. If not removed properly, these undesired resonances, when fed into the SQUID, can be amplified by the nonlinear current-voltage characteristic of the Josephson junctions, effectively compromising the performance of the SQUID [51–57].

The choice of the input-coil geometry is not arbitrary. Flux coupling is most efficient when the inductance of the input coil is (ignoring inductances of connecting lines) equal to the inductance of the pickup loop(s): $L_i = L_{PL}$ (if there are two electrically connected pickup loops then coupling is most efficient when $L_i = 2L_{PL}$). In this case, half of the sensed flux [flux through the pickup loop(s)] is screened by the pickup-loop portion of the input circuit and the other half by the coil at the input to the SQUID. Thus, the SQUID detects only a fraction of the external flux. The amount of flux detected by the SQUID, ϕ_s, depends on the mutual inductance between the input coil and the SQUID, M_i:

$$\phi_{PL}/\phi_s = 2L_i/M_i. \tag{3}$$

Generally, the mutual inductance is smaller than or equal to the input-coil self-inductance. Therefore, the flux noise performance (or energy sensitivity) of such a scheme is worse than that of the direct flux-coupling SQUID
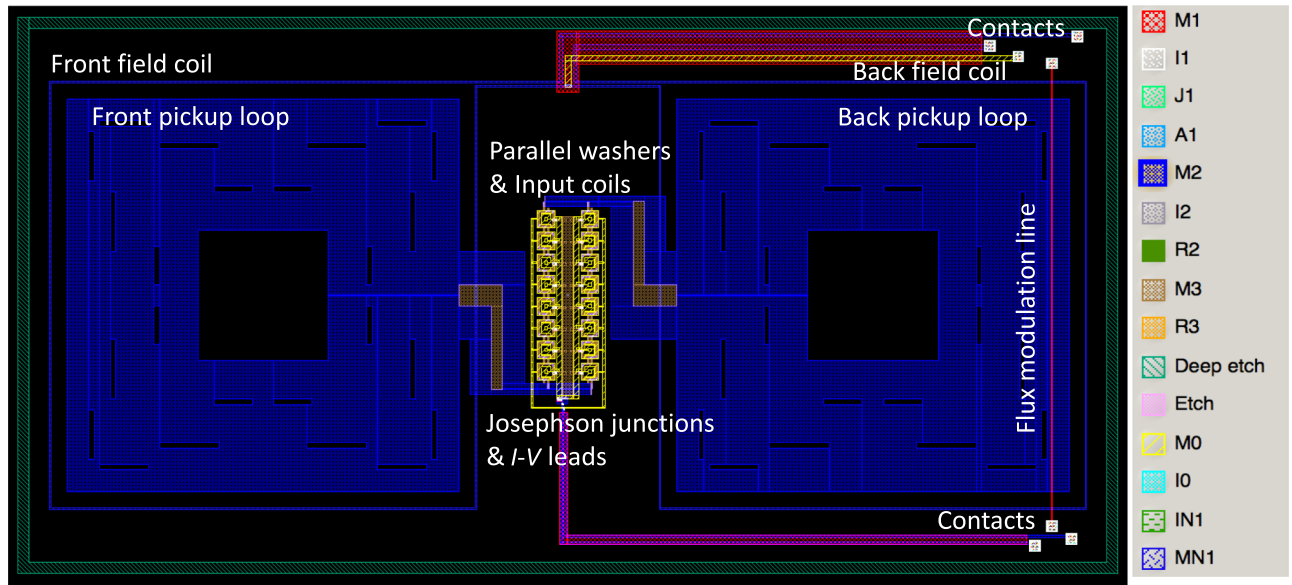
FIG. 6.   Representative design of a 100 aT gradiometric magnetometer and susceptometer. This image is a CAD layout with the main components labeled. Additional shield over washers not shown for clarity. Area of the image is 22×10.5 mm^2. See Appendix B for more details. In the legend, 'MN' and 'M' layers are niobium, 'IN' and 'I' layers are openings in the insulating layers, 'A' – anodization, 'J' – junctions area, 'R' – non-superconducting metal layers. The Layers correspond to the nomenclature used by Hypres Inc. and SeeQC, Inc.

described in Sec. I. However, a gain in field sensitivity may be obtained for much smaller pickup-loop sizes, because the effect on β is minimized with the input-coil scheme.

In other words, a practical benefit arises because the pickup loop can have a large inductance and a large flux-collection area without a large effect on the intrinsic noise: the input coil can be constructed to have a matching inductance, for example, by using the Ketchen coupling scheme of a spiral input coil to a wide-washer SQUID [39,40]. In this case, the self-inductance of the input coil scales with the square of the number of turns, $L_i \approx n^2 L$, while the mutual inductance scales as $M_i \approx nL$ [27,30,40]. Thus, the flux noise performance of such a scheme is

$$\phi_{\mathrm{PL}} = \frac{2L_i}{M_i}\phi_s = 2n\phi_s. \tag{4}$$

Combining Eq. (4) with the basic noise performance equation [Eq. (2)] reveals that the size of the SQUID for sensitivities in the range of 1 fT are substantially smaller than those in the direct-coupling schemes. This design, therefore, constitutes a promising direction to achieve high field sensitivities. In the next section, we discuss a further improvement with a scheme of several washers in parallel and input coils connected in series.

IV. ORIGINAL DESIGN WITH SERIES INPUT COILS AND FRACTIONAL SQUID LOOPS

The main advantage in using the field-coil input circuit is that the large inductance of the input coil can be

implemented without a substantial degradation of SQUID performance. However, the flux sensitivity is compromised during matching of the input-coil inductance and the pickup-loop inductance. This is tolerable for some applications, but often higher sensitivity is needed. Often, this compromise is forced by use of a commercial SQUID with a fixed-inductance input coil and a customer-provided pickup loop. In other words, when n is large in Eq. (4), it can degrade the performance of a standard input coil with the washer setup.

In the following approach, based on the "fractional SQUID" designs, we substantially improve this performance with parallel SQUID loops (Figs. 3 and 4). Instead of having one washer SQUID loop and an input coil consisting of many turns, we use many parallel washer SQUID loops [58], with a single-loop input coil each in the gradiometric configuration both for the pickup loops and the input washers to cancel out the influence of the external field noises, when the currents flow with opposite chirality in different subloops (Figs. 3 and 4). Each input loop is connected in series, and their parameters and the number of washers, N (and thus, the input-coil turns), are matched to the pickup-loop inductance. When using a single-turn coil, $n = 1$, per SQUID washer from Eqs. (3) and (4), assuming the same flux through all of the fractional washers, we obtain the total flux sensed by the SQUID as $\phi_s = (M_{1i}/2L_{1i})\phi_{\mathrm{PL}}/N$. For washers [39,40], the mutual inductance is equal to the washer inductance, $M_{1i} = L_1$ (Fig. 3), and therefore, $\phi_{\mathrm{PL}} = 2\phi_s$. This is the best flux-at-the-pickup to flux-at-the-SQUID

conversion that can be achieved. Our scheme presented here makes use of this estimate and opens up the possibility for femtotesla sensitivities within relatively small sizes of chips.

It is necessary to have on the order of $N = L_{\mathrm{PL}}/L$ SQUID loops connected in parallel, as well as the same number of input coils, leading to a total matching to the pickup-loop inductance of tens of nH. Figure 5 shows our calculations of these inductances for several target field sensitivities. The calculations are done by looping through w and D, calculating the expected SQUID flux noise given the inductances and other parameters of the SQUID and junctions, translating those to field noise using the effective area of the pickup loop, and then displaying lines of equal field noise as a function of the size of the pickup loop. Compellingly, this design promises subfemtotesla sensitivity in about 10×10 mm^2 footprint per pickup loop. This promises many additional uses in fields ranging from material sciences to neurosciences and in similar, or potentially more compact, experimental setups [59–70].

V. FABRICATION-READY GRADIOMETER FOR THE FEMTOTESLA RANGE

Gradiometric designs [71] can offer an external noise rejection of about 10 000 times or more [1,72–74]. In addition, gradiometers enable more efficient studies of material properties, as they are not susceptible to background signals that do not originate from the samples under study. A field coil can be used to induce local magnetization in the materials. Following the concepts and calculations proposed in the preceding sections, we design 50 fT gradiometers (and susceptometers) within about 10×20 mm^2 (Fig. 6).

Figure 6 depicts the overall layout, along with a legend for the layers legend. The pickup loops are wide, and therefore, have moats for flux trapping [75] to reduce the potential $1/f$ component (so other components of the SQUID have moats). This design implements 16 parallel washers, and the main geometries of the SQUID are summarized in Table I. Figure 7 in Appendix B contains details of one realization of the Josephson junctions' region

TABLE I. Geometrical parameters of a femtotesla SQUID gradiometer.

Component	Inner size, D (mm)	Line width, w (mm)	Nominal inductance (nH)	Screened inductance (nH)
Pickup loop	8.850	0.1	36.2	—
One input-coil turn	0.625	0.011	2.25	2.21
One SQUID washer	0.600	0.05	1.59	1.03

with shunt resistors and an additional damping resistor [52,76–79], which reflect the $\beta = 1$ condition for a 10 μA critical current with 16 parallel washers, resulting in about 100 pH SQUID inductance. Figure 8 in Appendix B illustrates a section that includes several parallel washer SQUIDs that are arranged in two parallel columns of eight. These washers have flux-trapping moats [75]. The first eight and remaining eight washers are also gradiometrically configured to reject external noise. The two sets of input coils are electrically isolated. Very small parasitic inductances, due to the wide lines, and very small capacitances, due to very thick oxide (a couple of micrometers of SiO$_2$), are achieved in these designs: the total parasitics are in the range of a few hundreds of pH. The undesired effects of these parasitics should be further minimized by the damping resistors. Figure 9 in Appendix B shows an individual 1.59 nH washer section, with the flux-trapping moats [75] and damping resistors emphasized. Overall, these designs show compact devices with greatly enhanced field sensitivity, while still being of similar or smaller dimensions than those previously reported [59–70]. This makes this design very attractive for practical applications, requiring only a few millimeters of spatial resolution and yielding an extraordinary field sensitivity in a potentially more compact form than that used before. Moreover, they can be manufactured at a foundry using conventional superconducting integrated-circuit fabrication methods.

VI. SUMMARY

Our detailed optimization methods yield gradiometric SQUID designs with projected sensitivities in the femtotesla range. Several variants of the designs can be implemented, mainly with varying pickup-loop dimensions and numbers of washers. Other parameters that can be varied marginally are the critical currents in Josephson junctions, as well as the quantity of such junctions and the values of their shunting resistors. These SQUIDs, even when gradiometric, are of a small size that are practical and relevant for use in various technological and scientific applications, where unprecedented field sensitivity is required. This potentially opens the door to beyond the femtotesla range, so that attotesla-sensitivity SQUID sensors can be fabricated as compact chips in the near future, which may open up technological capabilities for discoveries of various phenomena in quantum materials and in other interdisciplinary fields [48,80–86] of science and technology, including qubits and quantum information.

APPENDIX A: OPTIMIZING FLUX TRANSFER FOR N FRACTIONAL-LOOP SQUID AND IN-SERIES INPUT-COIL LOOPS

Here, we provide details that lead to the conclusion that the design with a fractional-loop SQUID with one-turn in-series input-coil loops is optimal for our purposes of detecting efficiently fluxes sensed by large inductance pickup loops, but with relatively small dimensions. When a flux, $\Delta\phi_{\mathrm{PL}}$, from a studied source couples to the pickup loop, it induces a screening current, J_i, which produces an equal amount of flux distributed in the input transformer, as follows [87]:

$$J_i L_{\mathrm{PL}} + J_i L_{i,\,\mathrm{eff}} + J_i L_{i,\,\mathrm{strip}} = \Delta\phi_{\mathrm{PL}},$$

where the effective screened inductance of the input coil with N one-turn loops [1] is

$$L_{i,\,\mathrm{eff}} \approx (1 - k_i^2 s)L_i = (1 - k_i^2 s)N L_{1i}.$$

The input-coil coupling constant is $k_i = (M_1/\sqrt{L_1 L_{1i}}) = \sqrt{L_1/L_{1i}}$; s is defined in Ref. [1] and is on the order of 0.04 in our example above, L_i is the total unscreened input-coil inductance, L_{1i} is the inductance of the unscreened one-input-coil segment of N connected in series, and M_1 is the mutual inductance between one segment of the input coil and one fractional SQUID washer.

In the classic washer geometry, the inductance of the input coil (an n-turn secondary coil) actually coupled to the washer (a one-turn wide primary coil) is equal to the washer inductance due to an almost perfect imaging of the secondary coil by currents in the primary coil plus the strip inductance of the secondary coil [1,30]:

$$L_{1i} = n^2 L_1 + n L_{1,\mathrm{strip}}.$$

The flux-transfer factor is the ratio between the externally applied pickup-loop flux, $\Delta\phi_{\mathrm{PL}}$, and the flux sensed by the SQUID, $\Delta\phi_s = M_1/N \times N J_i = k_i\sqrt{L_1 L_{1i}}J_i$ [30,87]:

$$F = \frac{k_i M_1 \sqrt{L_1 L_{1i}}}{L_{\mathrm{PL}} + (1 - k_i^2 s)N L_{1i}}.$$

By taking the derivative of this expression with respect to the pickup-loop inductance, it can be easily shown that this factor is maximized when $L_{\mathrm{PL}} = (1 - k_i^2 s)N L_{1i}$, yielding the maximum factor:

$$F_{\mathrm{max}} = \frac{k_i/N}{2\sqrt{(1 - k_i^2 s)}}\sqrt{\frac{L_1}{L_{1i}}},$$

Typically, for wide washers and narrow input coils fabricated with standard lithography, $k_i \approx 0.7 - 0.9$ and s is on

the level of a few percent [1], and therefore,

$$F_{\mathrm{max}} \approx \frac{1}{2N}\sqrt{\frac{L_1}{L_{1i}}}.$$

Inserting known expressions for the washer and the input-coil inductances [1,88] gives

$$F_{\mathrm{max}} \approx \frac{1}{2N}\sqrt{\frac{L_h + L_{\mathrm{SI}}}{n^2\left(L_h + \frac{L_{\mathrm{SI}}}{3}\right) + n L_{\mathrm{strip}}}},$$

L_h is the geometric inductance of the central hole in a washer (primary coil), L_{SI} is the slit inductance, and L_{strip} is the stripline inductance of the secondary line (which essentially represents flux leakage). In relatively large washers (tens or hundreds of μm), we can safely assume $L_h \gg L_{\mathrm{SI}}$ for finding the optimal n. Furthermore, in our case, L_{strip} is in the order of 100 pH per turn of the input coil, while $L_h \approx L = 1.59$ nH. We can thus write

$$F_{\mathrm{max}} \approx \frac{1}{2Nn},$$

which is obviously optimized for $n = 1$ and $L = 1$, as in our design (notably, this is not necessarily accurate for small SQUIDs, for example, with a larger fraction of flux leakage in between the primary and secondary soils and in the washer slit).

This result echoes textbook expressions for the classic input-coil design for a single washer [72,87], with the exception that our expression contains variables that represent a single segment in the input coil and a single turn in the fractional washer. Thus, in our case, the Josephson junctions will see a much smaller $(L_1/N)[1 - s_i k_i(N L_{1i}/N L_{1i} + L_{\mathrm{PL}})]$ inductance, $s_i = 0.5$ in our case, as defined in Ref. [1], which is beneficial for maintaining a relatively high overall energy sensitivity of the SQUID (meeting the optimization condition for $\beta = 1$).

Notably, also, the energy sensitivity of our design is not better than that of previous approaches and is still fundamentally limited by the same considerations as those in the classic cases [30,51,87], but this design is optimized for the compactness of the pickup loop, while maintaining a high integrated flux (field) sensitivity without compromising the SQUID inductance. There is one instructive way to understand our results, in that the flux from the pickup loop is effectively squeezed by a factor of about 100 (in our example) into a smaller area, while still being effectively coupled to a small-inductance SQUID. This effect may have further fundamental applications in quantum sensing, in general.
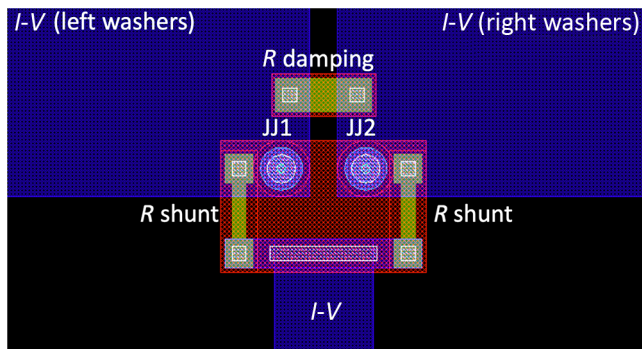
FIG. 7. Josephson junctions (JJ1 and JJ2). Area of the image is $45 \times 30 \ \mu m^2$. This design provides small parasitic inductance and resonance damping.

APPENDIX B: DETAILS OF THE DESIGN LAYOUT

Figures 7–9 are enlarged regions of the design presented in Fig. 6. They serve as examples of the design details to guide engineering efforts based on our paper.

APPENDIX C: ADDITIONAL MOTIVATIONS AND CONSIDERATIONS FOR SCANNED SQUID READOUT AND OTHER USES

If one would like to explore experimentally how coupling between a qubit and a readout squid influences the performance of the qubit, a SQUID, such as the one presented here, installed in a scanning apparatus will allow scanning over a large area of a wafer containing many quantum chips, and thus, effectively replace hundreds, if not more, on-chip fabricated read-out or diagnostics SQUID devices. In a scanning mode, different SQUID-qubit geometrical arrangements (couplings) can be explored more easily than that with on-chip readouts.

When a weak coupling is desired, one can think of a (flux) qubit as being a magnetic dipolelike source, where,
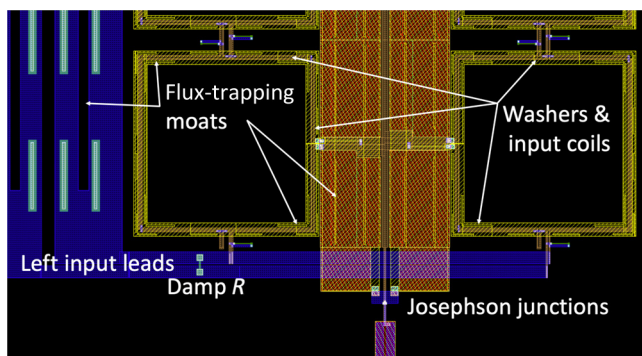

FIG. 8. Input coil and parallel washers. Area of the image is 2×1 mm^2. This is an approach with single-turn input coils connected in series, while the washers are connected in parallel to reduce the SQUID inductance.
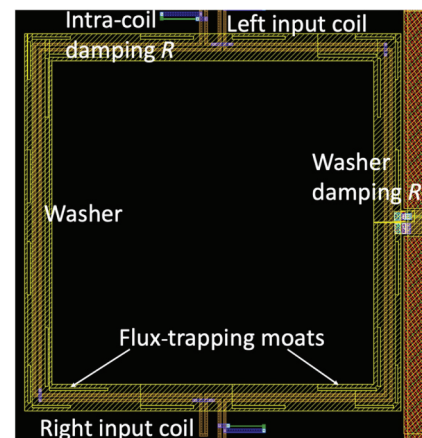

FIG. 9. Details of the washer section. One-turn loops are used as input coils: one coil for each of the gradiometer pickup loops. Flux traps are implemented as moats in wide Nb sections. Damping resistors are implemented.

in weak coupling, one would want to position the SQUID far enough away from the qubit. At the same time, the collected signal is lost, so to compensate for that, one would want to increase the detection area of the SQUID (to collect more flux). The back action of the noise from the large SQUID on the qubit is smaller than that of a small noisy SQUID coupled to a small qubit SQUID, as the noise is likely to be dispersed in many directions and not just directly in the qubit. Thus, the hypothesis is that a large fraction of the noise electromagnetic radiation will disperse in the open space (into a cavity and grounded cryostat parts), while a large fraction of the qubit signal can be collected by the large SQUID. More thorough calculations of back actions and experiments will be required to support this hypothesis in the future, but these are beyond the scope of this work. In addition, by implementing a remote SQUID, coupling of noise through the substrate to the qubit is eliminated, which, again, provides advantages for quantum diagnostics tools.

The kind of SQUIDs presented here could be useful for wafer-scale testing apparatuses for quantum-information technologies, similar to the one introduced recently by Bluefors-Intel-Afore, which is tagged a cryogenic wafer prober for the millikelvin range and said to dramatically help at speeding up the developments of cryogenic quantum devices [89]. Our sensors can enhance the capabilities of such diagnostics tools.

Another possibility for using these sensors is to test complex noisy quantum systems and to troubleshoot their performance. One such example is when targeting on the individual qubit level may not be useful due to the overall complexity of the tested chip, but the integrated sensitivity to noise and fluctuations is desired. In this case, the spatial resolution is compromised, but finer integrated field

resolution be obtained, allowing for *spectroscopic* studies of complex quantum systems.

---

[1] J. Clarke and A. I. Braginski, *The SQUID Handbook: Fundamentals and Technology of SQUIDs and SQUID Systems*, 1 Ed. (Wiley-VCH, Weinheim, 2004).

[2] José Martínez-Pérez Maria and Koelle Dieter, NanoSQUIDs: Basics & recent advances, Phys. Sci. Rev. **2,** 1 (2017).

[3] I. Sochnikov, A. J. Bestwick, J. R. Williams, T. M. Lippman, I. R. Fisher, D. Goldhaber-Gordon, J. R. Kirtley, and K. A. Moler, Direct measurement of current-phase relations in superconductor/topological insulator/superconductor junctions, Nano Lett. **13,** 3086 (2013).

[4] I. Sochnikov, L. Maier, C. A. Watson, J. R. Kirtley, C. Gould, G. Tkachov, E. M. Hankiewicz, C. Brüne, H. Buhmann, L. W. Molenkamp, and K. A. Moler, Nonsinusoidal Current-Phase Relationship in Josephson Junctions From the 3D Topological Insulator HgTe, Phys. Rev. Lett. **114,** 066801 (2015).

[5] Y. Frenkel, N. Haham, Y. Shperber, C. Bell, Y. Xie, Z. Chen, Y. Hikita, H. Y. Hwang, E. K. H. Salje, and B. Kalisky, Imaging and tuning polarity at $SrTiO_3$ domain walls, Nat. Mater. **16,** 1203 (2017).

[6] D. V. Christensen, Y. Frenkel, Y. Z. Chen, Y. W. Xie, Z. Y. Chen, Y. Hikita, A. Smith, L. Klein, H. Y. Hwang, N. Pryds, and B. Kalisky, Strain-tunable magnetism at oxide domain walls, Nat. Phys. **15,** 269 (2018).

[7] K. Bagani, J. Sarkar, A. Uri, M. L. Rappaport, M. E. Huber, E. Zeldov, and Y. Myasoedov, Sputtered $Mo_{66}Re_{34}$ SQUID-on-Tip for High-Field Magnetic and Thermal Nanoimaging, Phys. Rev. Appl. **12,** 044062 (2019).

[8] J. A. Bert, K. C. Nowack, B. Kalisky, H. Noad, J. R. Kirtley, C. Bell, H. K. Sato, M. Hosoda, Y. Hikita, H. Y. Hwang, and K. A. Moler, Gate-tuned superfluid density at the superconducting $LaAlO_3/SrTiO_3$ interface, Phys. Rev. B **86,** 060503 (2012).

[9] R. H. Koch, G. A. Keefe, F. P. Milliken, J. R. Rozen, C. C. Tsuei, J. R. Kirtley, and D. P. DiVincenzo, Experimental Demonstration of an Oscillator Stabilized Josephson Flux Qubit, Phys. Rev. Lett. **96,** 127001 (2006).

[10] S. Saito, T. Meno, M. Ueda, H. Tanaka, K. Semba, and H. Takayanagi, Parametric Control of a Superconducting Flux Qubit, Phys. Rev. Lett. **96,** 107001 (2006).

[11] M. G. Castellano, F. Chiarello, P. Carelli, C. Cosmelli, F. Mattioli, and G. Torrioli, Deep-well ultrafast manipulation of a SQUID flux qubit, New J. Phys. **12,** 043047 (2010).

[12] H. Deng, Y. Wu, Y. Zheng, N. Akhtar, J. Fan, X. Zhu, J. Li, Y. Jin, and D. Zheng, Working point adjustable DC-SQUID for the readout of Gap tunable flux qubit, IEEE Trans. Appl. Supercond. **25,** 1 (2015).

[13] X. Y. Jin, S. Gustavsson, J. Bylander, F. Yan, F. Yoshihara, Y. Nakamura, T. P. Orlando, and W. D. Oliver, Z-Gate Operation on a Superconducting Flux Qubit via its Readout SQUID, Phys. Rev. Appl. **3,** 034004 (2015).

[14] C. Eichler and J. R. Petta, Realizing a Circuit Analog of an Optomechanical System with Longitudinally Coupled Superconducting Resonators, Phys. Rev. Lett. **120,** 227702 (2018).

[15] E. Leonard, M. A. Beck, J. Nelson, B. G. Christensen, T. Thorbeck, C. Howington, A. Opremcak, I. V. Pechenezhskiy, K. Dodge, N. P. Dupuis, M. D. Hutchings, J. Ku, F. Schlenker, J. Suttle, C. Wilen, S. Zhu, M. G. Vavilov, B. L. T. Plourde, and R. McDermott, Digital Coherent Control of a Superconducting Qubit, Phys. Rev. Appl. **11,** 014009 (2019).

[16] X. Wang, A. Miranowicz, and F. Nori, Ideal Quantum Nondemolition Readout of a Flux Qubit Without Purcell Limitations, Phys. Rev. Appl. **12,** 064037 (2019).

[17] J. R. Kirtley, Fundamental studies of superconductors using scanning magnetic imaging, Rep. Prog. Phys. **73,** 126501 (2010).

[18] R. McDermott, M. G. Vavilov, B. L. T. Plourde, F. K. Wilhelm, P. J. Liebermann, O. A. Mukhanov, and T. A. Ohki. Quantum–classical interface based on single flux quantum digital logic, Quantum Sci. Technol. **3,** 024004 (2018).

[19] Notably, normally, on-chip dc SQUID can dampen the coherence of a qubit substantially, e.g., due to resistive shunts. Using a remote SQUID off a qubit chip and, at the same time, increasing the field integration (pickup) area may reduce such decoherence effects, as the mutual inductance decreases, while the effective signal-to-noise ratio may be increased with the SQUID pickup area.

[20] J. Aumentado, M. W. Keller, J. M. Martinis, and M. H. Devoret, Nonequilibrium Quasiparticles and 2e Periodicity in Single-Cooper-Pair Transistors, Phys. Rev. Lett. **92,** 066802 (2004).

[21] U. Patel, I. V. Pechenezhskiy, B. L. T. Plourde, M. G. Vavilov, and R. McDermott. Phonon-mediated quasiparticle poisoning of superconducting microwave resonators, Phys. Rev. B **96,** 220501 (2017).

[22] D. Drung and H. Koch, An integrated DC SQUID magnetometer with variable additional positive feedback, Supercond. Sci. Technol. **7,** 242 (1994).

[23] P. Kumar, S. Sendelbach, M. A. Beck, J. W. Freeland, Z. Wang, H. Wang, C. C. Yu, R. Q. Wu, D. P. Pappas, and R. McDermott, Origin and Reduction of $1/f$ Magnetic Flux Noise in Superconducting Devices, Phys. Rev. Appl. **6,** 041001 (2016).

[24] F. Yan, S. Gustavsson, A. Kamal, J. Birenbaum, A. P. Sears, D. Hover, T. J. Gudmundsen, D. Rosenberg, G. Samach, S. Weber, J. L. Yoder, T. P. Orlando, J. Clarke, A. J. Kerman, and W. D. Oliver, The flux qubit revisited to enhance coherence and reproducibility, Nat. Commun. **7,** 12964 (2016).

[25] L. B. Nguyen, Y.-H. Lin, A. Somoroff, R. Mencia, N. Grabon, and V. E. Manucharyan, High-Coherence fluxonium qubit, Phys. Rev. X **9,** 041041 (2019).

[26] C. D. Tesche and J. Clarke, Dc SQUID: Noise and optimization, J. Low Temp. Phys. **29,** 301 (1977).

[27] M. B. Ketchen, D. D. Awschalom, W. J. Gallagher, A. W. Kleinsasser, R. L. Sandstrom, J. R. Rozen, and B. Bumble, Design, fabrication, and performance of integrated miniature SQUID susceptometers, IEEE Trans. Magn. **25,** 1212 (1989).

[28] D. Drung, Introduction to Nb-based SQUID Sensors (2016), (available at https://snf.ieeecsc.org/abstracts/cr70-introduction-nb-based-squid-sensors).

[29] H. Weinstock, Ed., *SQUID Sensors: Fundamentals, Fabrication and Applications* (Springer Netherlands, 1996), Nato Science Series E.

[30] M. Ketchen, DC SQUIDs 1980: The state of the art, IEEE Trans. Magn. **17,** 387 (1981).

[31] P. Carelli and M. G. Castellano, High-sensitivity DC-SQUID measurements, Phys. B Condens. Matter **280,** 537 (2000).

[32] F. Giazotto, J. T. Peltonen, M. Meschke, and J. P. Pekola, Superconducting quantum interference proximity transistor, Nat. Phys. **6,** 254 (2010).

[33] A. Ronzani, C. Altimiras, and F. Giazotto, Highly Sensitive Superconducting Quantum-Interference Proximity Transistor, Phys. Rev. Appl. **2,** 024005 (2014).

[34] J. R. Kirtley, L. Paulius, A. J. Rosenberg, J. C. Palmstrom, C. M. Holland, E. M. Spanton, D. Schiessl, C. L. Jermain, J. Gibbons, Y.-K.-K. Fung, M. E. Huber, D. C. Ralph, M. B. Ketchen, G. W. Gibson, and K. A. Moler, Scanning SQUID susceptometers with sub-micron spatial resolution, Rev. Sci. Instrum. **87,** 093702 (2016).

[35] R. N. Jabdaraghi, D. S. Golubev, J. P. Pekola, and J. T. Peltonen, Noise of a superconducting magnetic flux sensor based on a proximity Josephson junction, Sci. Rep. **7,** 8011 (2017).

[36] S. M. Anton, J. S. Birenbaum, S. R. O'Kelley, V. Bolkhovsky, D. A. Braje, G. Fitch, M. Neeley, G. C. Hilton, H.-M. Cho, K. D. Irwin, F. C. Wellstood, W. D. Oliver, A. Shnirman, and J. Clarke, Magnetic Flux Noise in dc SQUIDs: Temperature and Geometry Dependence, Phys. Rev. Lett. **110,** 147002 (2013).

[37] J. A. B. Mates, K. D. Irwin, L. R. Vale, G. C. Hilton, and H. M. Cho, An efficient superconducting transformer design for SQUID magnetometry, J. Low Temp. Phys. **176,** 483 (2014).

[38] H. Seppa, T. Ryhanen, R. Imoniemi, and J. Knuutila, *Superconducting Technology: 10 Case Studies* (World Scientific, New York, 1991), pp. 1–29.

[39] M. B. Ketchen and J. M. Jaycox, Ultra-low-noise tunnel junction dc SQUID with a tightly coupled planar input coil, Appl. Phys. Lett. **40,** 736 (1982).

[40] J. Jaycox and M. Ketchen, Planar coupling scheme for ultra low noise DC SQUIDs, IEEE Trans. Magn **17,** 400 (1981).

[41] T. Van Duzer and C. Terner, *Principles of Superconductive Devices and Circuits*, 2nd Ed. (Prentice-Hall PTR, Upper Saddle River, N.J, 1999).

[42] E. H. Brandt, Thin superconductors and SQUIDs in perpendicular magnetic field, Phys. Rev. B **72,** 024529 (2005).

[43] M. B. Ketchen, K. G. Stawiasz, D. J. Pearson, T. A. Brunner, C-K Hu, M. A. Jaso, M. P. Manny, A. A. Parsons, and K. J. Stein, Sub-μm linewidth input coils for low Tc integrated thin-film dc superconducting quantum interference devices, Appl. Phys. Lett. **61,** 336 (1992).

[44] P. Carelli and V. Foglietti, Improved multi-loop DC SQUID, IEEE Trans. Magn **19,** 299 (1983).

[45] S. Zarembiński and T. Claeson, Design of multiloop input circuits for high-T_c superconducting quantum interference magnetometers, J. Appl. Phys. **72,** 1918 (1992).

[46] D. Drung, S. Knappe, and H. Koch, Theory for the multiloop dc superconducting quantum interference device

magnetometer and experimental verification, J. Appl. Phys. **77,** 4088 (1995).

[47] M. Kiviranta, L. Gronberg, and J. Hassel, A multiloop SQUID and a SQUID array With 1-μm and submicrometer input coils, IEEE Trans. Appl. Supercond. **22,** 1600105 (2012).

[48] J. Luomahaara, A. Kemppinen, P. Helistö, and J. Hassel, Characterization of SQUID-based null detector for a quantum metrology triangle experiment, IEEE Trans. Appl. Supercond. **23,** 1601705 (2013).

[49] J. Luomahaara, M. Kiviranta, L. Grönberg, K. C. J. Zevenhoven, and P. Laine, Unshielded SQUID sensors for ultra-Low-field magnetic resonance imaging, IEEE Trans. Appl. Supercond. **28,** 1 (2018).

[50] M. Kiviranta, L. Grönberg, J. van der Kuur, Two SQUID amplifiers intended to alleviate the summing node inductance problem in multiplexed arrays of Transition Edge Sensors. arXiv:1810.09122 (2018) (available at arxiv.org/abs/1810.09122).

[51] J. Knuutila, M. Kajola, H. Seppä, R. Mutikainen, and J. Salmi, Design, optimization, and construction of a dc SQUID with complete flux transformer circuits, J. Low Temp. Phys. **71,** 369 (1988).

[52] V. Foglietti, W. J. Gallagher, M. B. Ketchen, A. W. Kleinsasser, R. H. Koch, and R. L. Sandstrom, Performance of dc SQUIDs with resistively shunted inductance, Appl. Phys. Lett. **55,** 1451 (1989).

[53] K. Enpuku and K. Yoshida, Modeling the dc superconducting quantum interference device coupled to the multiturn input coil, J. Appl. Phys. **69,** 7295 (1991).

[54] T. Ryhanen, R. Cantor, D. Drung, H. Koch, and H. Seppa, Effect of parasitic capacitance on DC SQUID performance, IEEE Trans. Magn **27,** 3013 (1991).

[55] V. Foglietti, M. E. Giannini, and G. Petrocco, A double DC-SQUID device for flux locked loop operation, IEEE Trans. Magn **27,** 2989 (1991).

[56] R. Cantor, K. Enpuku, T. Ryhanen, and H. Seppa, A high performance integrated DC SQUID magnetometer, IEEE Trans. Appl. Supercond. **3,** 1800 (1993).

[57] M. E. Huber, P. A. Neil, R. G. Benson, D. A. Burns, A. M. Corey, C. S. Flynn, Y. Kitaygorodskaya, O. Massihzadeh, J. M. Martinis, and G. C. Hilton, DC SQUID series array amplifiers with 120 MHz bandwidth, IEEE Trans. Appl. Supercond. **11,** 1251 (2001).

[58] P. Carelli, M. G. Castellano, G. Torrioli, and R. Leoni, Low noise multiwasher superconducting interferometer, Appl. Phys. Lett. **72,** 115 (1998).

[59] R. Ilmoniemi, J. Knuutila, T. Ryhänen, and H. Seppä, in *Progress in Low Temperature Physics*, edited by D. F. Brewer (Elsevier, Amsterdam, 1989), Vol. 12, pp.271–339.

[60] W. Vodel and K. Makiniemi, An ultra low noise DC SQUID system for biomagnetic research, Meas. Sci. Technol. **3,** 1155 (1992).

[61] D. Drung and H. Koch, An electronic second-order gradiometer for biomagnetic applications in clinical shielded rooms, IEEE Trans. Appl. Supercond. **3,** 2594 (1993).

[62] C. Granata, A. Vettoliere, and M. Russo, Miniaturized superconducting quantum interference magnetometers for high sensitivity applications, Appl. Phys. Lett. **91,** 122509 (2007).

[63] C. Granata, A. Vettoliere, S. Rombetto, C. Nappi, and M. Russo, Performances of compact integrated superconducting magnetometers for biomagnetic imaging, J. Appl. Phys. **104**, 073905 (2008).

[64] M. I. Faley, U. Poppe, K. Urban, and R. L. Fagaly, Noise analysis of DC SQUIDs with damped superconducting flux transformers, J. Phys. Conf. Ser. **234**, 042009 (2010).

[65] A. Vettoliere, C. Granata, S. Rombetto, and M. Russo, Modeled performance of a long baseline planar SQUID gradiometer for biomagnetism, IEEE Trans. Appl. Supercond. **21**, 383 (2011).

[66] Y. Zhang, C. Liu, M. Schmelz, H.-J. Krause, A. I. Braginski, R. Stolz, X. Xie, H.-G. Meyer, A. Offenhäusser, and M. Jiang, Planar SQUID magnetometer integrated with bootstrap circuitry under different bias modes, Supercond. Sci. Technol. **25**, 125007 (2012).

[67] A. Tsukamoto, S. Adachi, Y. Oshikubo, and K. Tanabe, Design and fabrication of directly-coupled HTS-SQUID magnetometer With a multi-turn input coil, IEEE Trans. Appl. Supercond. **23**, 1600304 (2013).

[68] K. Yang, H. Chen, X. Kong, L. Lu, M. Li, R. Yang, and X. Xie, Weakly damped SQUID gradiometer With Low crosstalk for magnetocardiography measurement, IEEE Trans. Appl. Supercond. **26**, 1 (2016).

[69] M. Schmelz, V. Zakosarenko, A. Chwala, T. Schönau, R. Stolz, S. Anders, S. Linzen, and H. Meyer, Thin-film-based ultralow noise SQUID magnetometer, IEEE Trans. Appl. Supercond. **26**, 1 (2016).

[70] J.-H. Storm, P. Hömmen, D. Drung, and R. Körber, An ultra-sensitive and wideband magnetometer based on a superconducting quantum interference device, Appl. Phys. Lett. **110**, 072603 (2017).

[71] C. Granata and A. Vettoliere, Nano superconducting quantum interference device: A powerful tool for nanoscale investigations, Phys. Rep. **614**, 1 (2016).

[72] M. B. Ketchen, Design of improved integrated thin-film planar dc SQUID gradiometers, J. Appl. Phys. **58**, 4322 (1985).

[73] A. Kittel, K. A. Kouznetsov, R. McDermott, B. Oh, and J. Clarke, High T_c superconducting second-order gradiometer, Appl. Phys. Lett. **73**, 2197 (1998).

[74] A. Chwala, J. Kingman, R. Stolz, M. Schmelz, V. Zakosarenko, S. Linzen, F. Bauer, M. Starkloff, M. Meyer, and H.-G. Meyer, Noise characterization of highly sensitive SQUID magnetometer systems in unshielded environments, Supercond. Sci. Technol. **26**, 035017 (2013).

[75] M. Jeffery, T. Van Duzer, J. R. Kirtley, and M. B. Ketchen, Magnetic imaging of moat-guarded superconducting electronic circuits, Appl. Phys. Lett. **67**, 1769 (1995).

[76] K. Enpuku, T. Muta, K. Yoshida, and F. Irie, Noise characteristics of a dc SQUID with a resistively shunted inductance, J. Appl. Phys. **58**, 1916 (1985).

[77] K. Enpuku, K. Yoshida, and S. Kohjiro, Noise characteristics of a dc SQUID with a resistively shunted inductance. II. optimum damping, J. Appl. Phys. **60**, 4218 (1986).

[78] K. Enpuku and H. Koch, Washer resonances of DC superconducting quantum interference device coupled to multiturn input coil, Jpn. J. Appl. Phys. **32**, 3811 (1993).

[79] N. Shimizu, T. Morooka, and K. Enpuku, Suppression of washer resonance of DC superconducting quantum interference device by using New washer with additional slit, Jpn. J. Appl. Phys. **33**, L1215 (1994).

[80] J. Flokstra, H. J. M. Ter Brake, E. P. Houwman, D. Veldhuis, W. Jaszczuk, M. Caspari, H. Rogalla, A. Martínez, and C. Rillo, A 19-channel d.c. SQUID magnetometer system for brain research, Sens. Actuators Phys. **27**, 781 (1991).

[81] K. Isawa, S. Nakayama, M. Ikeda, S. Takagi, S. Tosaka, and N. Kasai, Robotic 3D SQUID imaging system for practical nondestructive evaluation applications, Phys. C Supercond. **432**, 182 (2005).

[82] C. Granata, A. Vettoliere, and M. Russo, An ultralow noise current amplifier based on superconducting quantum interference device for high sensitivity applications, Rev. Sci. Instrum. **82**, 013901 (2011).

[83] A. Chwala, J. P. Smit, R. Stolz, V. Zakosarenko, M. Schmelz, L. Fritzsch, F. Bauer, M. Starkloff, and H.-G. Meyer, Low temperature SQUID magnetometer systems for geophysical exploration with transient electromagnetics, Supercond. Sci. Technol. **24**, 125006 (2011).

[84] V. Zakosarenko, M. Schmelz, R. Stolz, T. Schönau, L. Fritzsch, S. Anders, and H.-G. Meyer, Femtoammeter on the base of SQUID with thin-film flux transformer, Supercond. Sci. Technol. **25**, 095014 (2012).

[85] M. I. Faley, J. Dammers, Y. V. Maslennikov, J. F. Schneiderman, D. Winkler, V. P. Koshelets, N. J. Shah, and R. E. Dunin-Borkowski, High-T_c SQUID biomagnetometers, Supercond. Sci. Technol. **30**, 083001 (2017).

[86] C. Granata, A. Vettoliere, O. Talamo, P. Silvestrini, R. Rucco, P. P. Sorrentino, F. Jacini, F. Baselice, M. Liparoti, A. Lardone, and G. Sorrentino, in *Sensors*, edited by B. Andò, F. Baldini, C. Di Natale, V. Ferrari, V. Marletta, G. Marrazza, V. Militello, G. Miolo, M. Rossi, L. Scalise, P. Siciliano (Springer International Publishing, Cham, Switzerland, 2019), pp. 203–209.

[87] J. O. Lekkala and J. A. V. Malmivuo, Optimization of a squid vector gradiometer, Cryogenics **25**, 291 (1985).

[88] M. B. Ketchen, Design considerations for DC SQUIDs fabricated in deep sub-micron technology, IEEE Trans. Magn **27**, 2916 (1991).

[89] Intel drives development of quantum cryoprober with Bluefors and Afore to accelerate quantum computing. *Intel Newsroom* (2019).